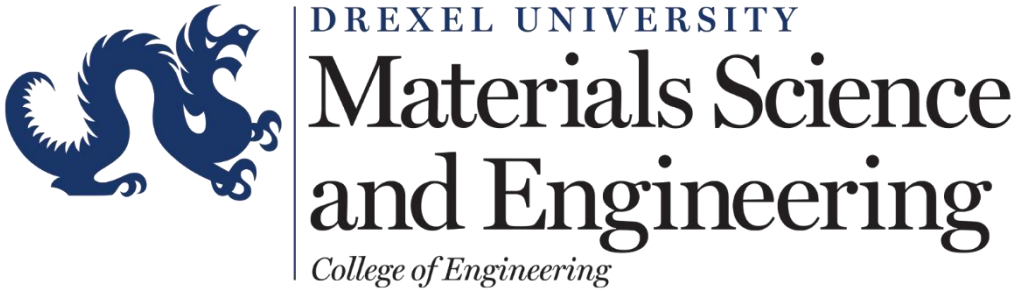

MATE 491
Fall 2017

Senior Design Project Fall Report: Fluorination of Manganese Oxide Nanostructures for Lithium-Ion Batteries

Mahidi Hassan, Sam Kulesa, and Geoffrey Xiao

Advisors: Dr. Ekaterina Pomerantseva & Dr. Steven May
Mentors: Bryan Byles & Jiayi Wang

Submitted December 7th, 2017

Problem Statement and Background

Since their 1980's debut, lithium-ion batteries have become integral to twenty-first century life. Lithium-ion battery technology has enabled enormous developments in consumer electronics, electric vehicles, and grid-level electrical storage. At the same time, many innovations are being stifled by the limits of current energy storage technology.

A typical battery (Figure 1a) consists of a negatively-charged anode coupled with a positively-charged cathode. Once the anode and cathode are electronically connected, electrons will flow from the anode to the cathode, generating current that can power a device. Accompanying the electron movement is lithium ion extraction from the anode and intercalation into the cathode. An electrolyte enables ionic diffusion, and this process continues until no more electrons can move from the anode to the cathode. In a secondary—or "reversible"—battery, a reversal of current can pull electrons back from the cathode to the anode and re-intercalate the lithium ions into the anode.

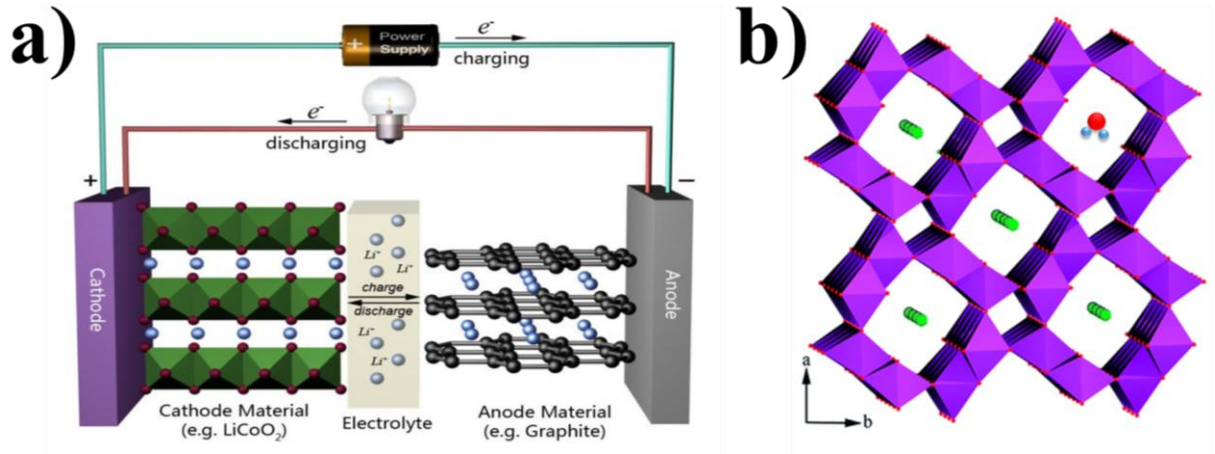

Figure 1. a) Conventional Li-ion battery. Adapted from School of Chemical Sciences, University of Illinois. http://www.scs.illinois.edu/murphy/Ran/research/energystorage.html. **b)** Crystal structure of α-MnO_2 showing stabilizing water molecules and potassium cations. Red: oxygen atoms. Purple octahedral surround the manganese atom. Green: potassium (K^+) ion. Blue: hydrogen atoms [1].

Early reversible batteries included lead-acid and nickel-cadmium. But what makes lithium-ion batteries so outstanding is its energy density and volumetric capacity: li-ion batteries can hold much more charge than other batteries, and have other advantages such as lower self-discharge and long cycling lifetime. A typical lithium-ion battery (Figure 1a) features a lithiated-graphite anode and nickel- or cobalt-based oxides, such as $LiCoO_2$, as a cathode.

The demand for these lithium-ion batteries continues increasing, and scientists and analysts alike have warned that the supplies of common materials in lithium-ion batteries are not limitless. Based on all accessible reserves in 2015, it was calculated that the world's current usage of lithium could be sustained for another 365 years [2]. But as the material consumption exponentially increases, the expected 365 years of lithium reserves may last as few as seventeen years [3].

Likewise, cobalt, nickel, and graphite are in limited supply or only abundant in areas with volatile supply chains [3]. The electrochemical properties of these materials are also hindrances. For example, per calculations with *Equation 1* (in Appendix), the theoretical maximum capacity of $LiCoO_2$, one of the most common cathodes, is 273 $mAhg^{-1}$. Similarly, another common cathode, $LiFePO_4$ has a theoretical capacity of 170 $mAHg^{-1}$. In practice, the capacity of these cathode materials is even less. The challenges in lithium-ion technology are not only supply-related, but based in properties as well.

A relatively new candidate for lithium-ion battery cathodes is α-MnO_2, an allotrope of MnO_2. α-MnO_2 forms tunnel-like nanowires, through which lithium ions can travel (Figure 1b). In addition to the tunnel structures providing ample space for lithium insertion and removal, water molecules and potassium ions occupy approximately ~87% of the tunnels to stabilize the structure. A major advantage for α-MnO_2 is that manganese is much more abundant than other cathode materials and is found in a diverse group of economically-stable locations [4]. Moreover, α-MnO_2 has shown promising performance with a theoretical capacity of 308 $mAhg^{-1}$ (Equation 1, Appendix) and good electrical properties [5]. There has also been research into using α-MnO_2 for beyond-lithium batteries based on sodium-ions [6]. The main roadblock for α-MnO_2, however, is its low capacity retention. α-MnO_2 cathodes quickly lose their capacity after a relatively low number of charge/discharge cycles, rendering them useless for applications in consumer electronics or electric vehicles which require capacity retention across thousands of charge/discharge cycles [7].

The aim of this project is to increase cyclability of energy storage devices utilizing α-MnO_2. This will be achieved through fluorination—the process of adding into or associating fluorine with α-MnO_2.

Rationale

One theorized reason for the low cyclability of α-MnO_2 is dissociation of Mn^{2+} from the lattice during repeated cycling and structural instabilities due to repeated lithiations and delithiations [8]. While the tunnels provide ample space for lithium insertion and removal, repeated lithiations/delithations can change the lattice structure and even induce phase transformations [9]. It is thought that F-Mn produces a stronger bond than O-Mn, thereby enhancing the structural integrity after repeated charge/discharge cycles [10]. Fluorination has also been used in many related manganese-based cathode materials to improve capacity retention (Figure 2). Figure 2 shows the discharge ratio: the discharge capacity of fluorinated material divided by discharge capacity of un-fluorinated material. The discharge ratios are greater than one and increasing with cycle number. For many of these materials, a fluorination (i.e *x* in $LiMO_{2-x}F_x$) as 0.02 has caused dramatic improvements in cycling performance.

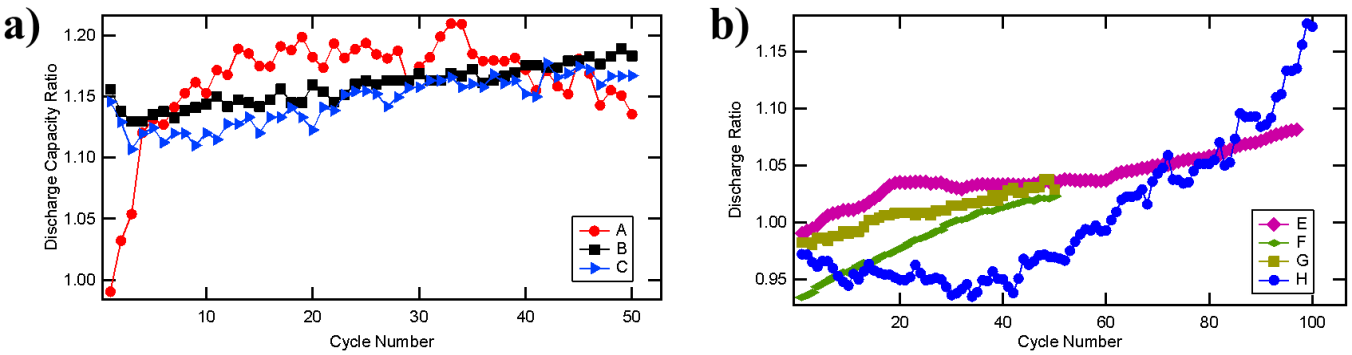

Figure 2. Discharge ratio is defined as the discharge capacity of the fluorinated material divided by the discharge capacity of the un-fluorinated material. A-C **(a)** are LiM_2O_4 spinel type and E-H **(b)** are layered $LiMO_2$ type materials[1].

The α-MnO_2 crystal structure is shown in Figure 1b. In a battery, upon discharge, lithium ions move from the anode and to the α-MnO_2 nanowires in the cathode. The unit cell of the α-MnO_2 allows lithium ions to travel through, or diffuse down, the structure: this combination of 1D crystal structure and 1D morphology simplifies the lithium-ion's access and diffusion process. α-

[1] A is $LiMn_2O_4$ / $LiMn_2O_{3.98}F_{0.08}$, B is $LiMn_{1.8}Li_{0.2}O_4$ / $LiMn_{1.8}Li_{0.2}O_{3.88}F_{0.12}$, C is $Li[Mn_{1.8}Li_{0.1}Ni_{0.1}]O_4$ / $Li[Mn_{1.8}Li_{0.1}Ni_{0.1}]O_{3.9}F_{0.1}$ [18]. E is $LiNi_{0.5}Mn_{1.5}O_4$ / $LiMn_{1.5}Ni_{0.5}O_4$ / $LiMn_{1.5}Ni_{0.5}O_{3.9}F_{0.1}$ [17]. F is $Li[Ni_{1/3}Co_{1/3}Mn_{1/3}]O_2$ / $Li[Ni_{1/3}Co_{1/3}Mn_{1/3}]O_{1.95}F_{0.05}$ [26]. G is $Li[Ni_{0.6}Co_{0.2}Mn_{0.2}]O_2$ / $Li[Ni_{0.6}Co_{0.2}Mn_{0.2}]O_{1.98}F_{0.02}$ [27]. H is $Li[Ni_{0.8}Co_{0.1}Mn_{0.1}]O_2$ / $Li[Ni_{0.8}Co_{0.1}Mn_{0.1}]O_{1.98}F_{0.02}$ [9].

MnO_2 is also synthesized as a nanowire, increasing surface area and the opportunities for lithium ion intercalation and extraction. There has been much work on cation doping in lithium intercalation electrodes, in which the transition metal is exchanged with similar transition metal ions. Cation-doping of the seminal $LiCoO_2$ has led to alternatives such as $LiNi_{0.5}Co_{0.5}O_2$ [11]. Similarly mixed cation manganese-based materials such as $LiNi_{0.5}Mn_{0.5}O_2$ have been produced to optimize electrochemical performance and stability by reducing problems such as Mn^{2+} dissolution [12]. Anion-doping on the other hand, has not been as systematically investigated. The fluorination of α-MnO_2 is expected to substitute in fluorine anions for oxygen anions, giving $MnO_{2-x}F_x$. Despite their potential, anion exchanges have not been as researched extensively as cation exchanges.

Goals and Objectives

The goal of this project is to investigate whether fluorination is a viable strategy to enhance α-MnO_2's electrochemical energy storage performance. Assigning specific quantitative targets is difficult because there are many free variables—the choice of anode, the electrolyte, test conditions, and more.

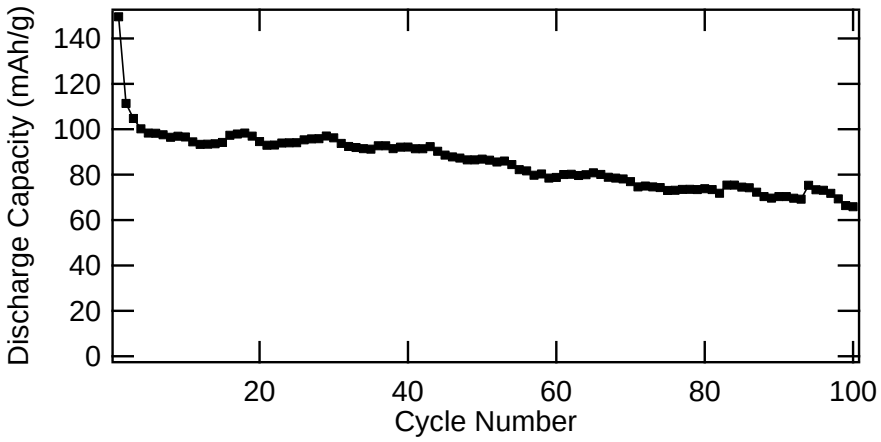

Figure 3. Discharge capacity cycling results for α-MnO_2 [13].

Previous data on α-MnO_2 (Figure 3) from the Materials Electrochemistry Group (MEG) at Drexel University (PI: Dr. Pomerantseva) shows that after 100 cycles, the discharge capacity decreases by more than 50%. Improving upon this result, and achieving closer to 70% capacity after 100 cycles with the same testing method is a desirable and realistic achievement. It is also important that the increases in capacity retention are not at the cost of capacity losses. Likewise,

the goal of this project is to do basic research into the effects of fluorination on crystal structure and material properties. In additional to electrochemical tests, magnetic property testing will be done to elucidate the complex interplay between composition, structure, and physical properties.

Experimental Approach

Synthesis of α-MnO_2 nanowires is performed using a high-pressure, hydrothermal method [14]. 1 mmol $KMnO_4$ and 1 mmol of NH_4Cl are dissolved in 20 mL of de-ionized water. A 23 mL Teflon-lined autoclave is filled with the solution and heated to 150°C for 24 hours [14]. The resulting powder product is filtered, rinsed, and ground, and then dried at 100°C for several hours to remove excess water. The synthesized product is K_xMnO_2, with x ~ 0.13%. The K^+ ions are confined within the tunnels to stabilize the crystal structure.

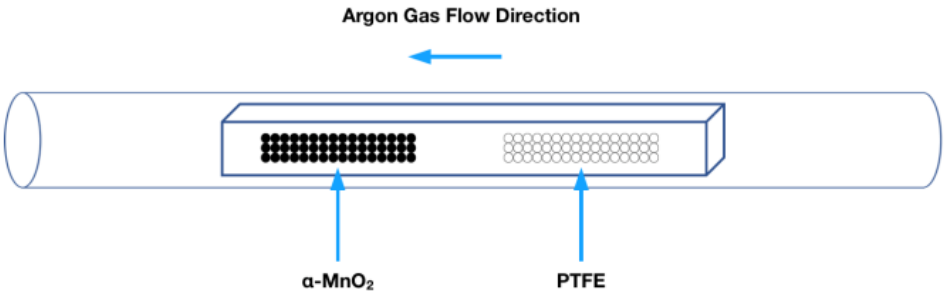

Figure 4. Vapor Transport Process.

A vapor transport method is used for the fluorination experiments [15], [16]. A schematic of this method can be seen in Figure 4. Essentially, α-MnO_2 and a fluorine source, polytetrafluoroethylene (PTFE), are placed in a ceramic boat, separated by aluminum foil so there is no physical contact between the α-MnO_2 and PTFE. The entire boat is also wrapped with aluminum foil to ensure the containment of fluorine. The boat is then placed within a glass tube which is heated to various temperatures and time durations using a ThermoFisher Lindberg Blue M Furnace. Argon gas is flown through the tube to carry the fluorine to react with the α-MnO_2. The two main fluorination parameters are time and temperature. An experimental matrix of the different fluorination temperatures and times can be seen in Table 1.

Table 1. List of experimental parameters.

Fluorination Parameters					
Run	Time (Hours)	Temperature (°C)	Fluorine Source	Gas Flow (Ar, sccm)	Complete?
1	4	380	PTFE	1/4	Yes
2	4	280	PTFE	1/4	Yes
3	4	180	PTFE	1/4	Yes
4	12	380	PTFE	1/4	Yes
5	12	280	PTFE	1/4	Yes
6	12	180	PTFE	1/4	Yes
7	24	380	PTFE	1/4	Yes
8	24	280	PTFE	1/4	Yes
9	24	180	PTFE	1/4	No
10	4	180	Pristine Sample	1/4	Yes
11	4	180	Non-fluoro Polymer	1/4	No

Control experiments will be done with polyethylene, a non-fluoropolymer, and with no polymer. Polyethylene is a good control experiment because it has a very similar structure to PTFE. These experiments will be conducted to ensure that the fluorine is what causes the property changes in α-MnO_2, and not the heat treatment or organic polymer. So far, temperatures of 180-380°C have been used for time lengths of 4, 12, and 24 hours. These temperatures and times are chosen based on equipment availability and thermal stability of α-MnO_2 and PTFE. Other fluorination methods have used high temperatures past 600°C, and between 5 and 20 hours [17], [18]. However, α-MnO_2 has lower thermal stability than these other oxide materials, as seen in the thermal gravimetric data in Figure 5: Retained water loss is seen ~200°C and significant decomposition is seen near ~600°C. PTFE thermal properties have also been considered, as it begins decomposition near 260°C and severely degrades at 400°C [19].

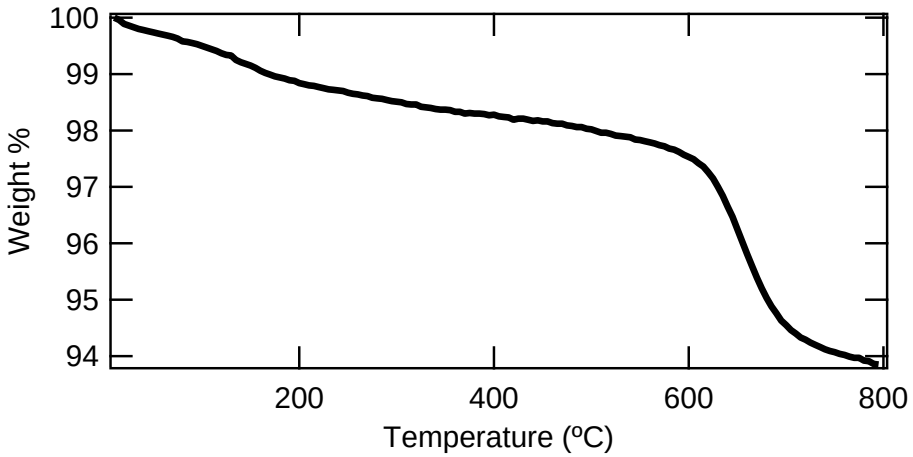

Figure 5. Thermogravimetric Analysis (TGA) of α -MnO_2 [13].

To measure the effects of fluorination and elucidate the impact of fluorination processing time and temperature, x-ray diffraction (XRD) will be conducted on all samples. To confirm fluorination and evaluate chemical composition, it was planned to use energy-dispersive X-ray spectroscopy (EDS). However, EDS has so far been inconclusive, as the manganese peak is extremely close to the fluorine peak (see *Results* section). Thus, it will be more effective to use x-ray photoelectron spectroscopy (XPS). XPS has commonly been used in fluorination research, and the fluorine 1s peak (~685 eV) should not overlap with the manganese (~641 eV) or oxygen peaks (~530 eV) [9], [17], [18]. XPS will also measure oxidation states, and can be paired with sputtering to measure depth profiles of chemical composition.

After confirming fluorination, electrochemical testing will be used to test the performance of fluorinated α-MnO_2. Primarily, charge-discharge cycles will be run with lithium anodes and liquid electrolytes, as per industry best-practices or standards from *SAE International* such as J-3159 (*Techniques for measuring the properties of lithium and lithium-ion battery anode active materials*) or J-3021-201410 (*Recommended Practice for Determining Material Properties of Li-Battery Cathode Active Materials*) to find the initial capacity and cyclability. Further electrochemical testing will include rate capability tests, which contribute to maximum charging speeds, and cyclic voltammetry, which tests reversibility and stability.

To verify results, once the optimal fluorination parameters have been identified, the experiments including fluorination, characterization, and testing will be repeated to ensure certainty in the results. Vibrating-sample magnetometry using a physical property measuring system (PPMS) will also be performed to determine the influence of fluorination on magnetic properties.

Additional ASTM standards will be consulted throughout the project. Due to the need for XPS chemical composition analysis, ASTM E995 *Standard Guide for Background Subtraction Techniques in Auger Electron Spectroscopy and X-Ray Photoelectron Spectroscopy* will be used. In brief, the standard provides invaluable information for the appropriate methods of analyzing XPS data and extracting quantitative information on chemical composition. Another useful ASTM standard is ASTM E2529 *Standard Guide for Testing the Resolution of a Raman Spectrometer*. Though Raman spectroscopy is not currently a main focus, Raman can be used to glean important structural properties [20]. Lastly, ASTM G106 *Standard Practice for Verification of Algorithm and Equipment for Electrochemical Impedance Measurements* may be used once the ideal

fluorination parameters have been identified and rigorous electrochemical impedance characterization is necessary.

Results and Discussion

First, the synthesis of un-fluorinated, pristine nanowire α-MnO_2 is confirmed. The nanowire morphology is desirable due to its high surface area for lithium ion intercalation and low dimensionality enabling un-impeded lithium ion diffusion. The nanowire morphology is confirmed using a Zeiss Supra 50 VP scanning electron microscopy (SEM) (Figure 6a). Powder x-ray diffraction (XRD) patterns were also obtained with a Rigaku SmartLab using the Cu $k\alpha_1$ and $k\alpha_2$ lines. The XRD patterns were indexed according to a I4/m space group and lattice parameters were found using the WinCSD software [21]. The XRD patterns (Figure 6b) likewise confirms the crystalline structure (PDF#01-077-1796) and the absence of second phases [14], [20]. All error bars in the accompanying figures represent one standard deviation (*Error Propagation*, Appendix).

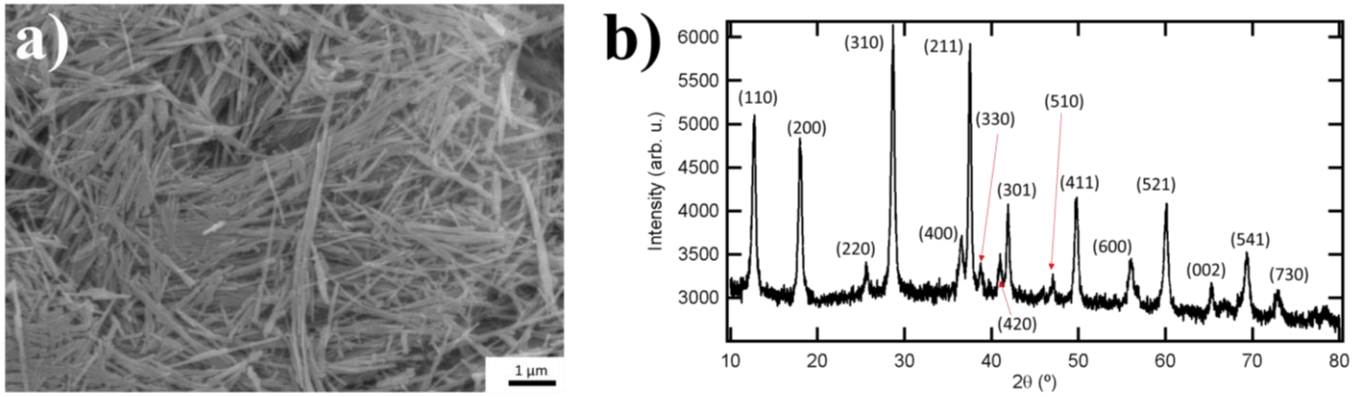

Figure 6. a) SEM confirms the nanowire morphology. **b)** XRD confirms the tetragonal I4/m crystalline structure of α-MnO_2. No secondary phases are detected.

To determine the fluorine incorporation, energy-dispersive X-ray spectroscopy (EDS) was performed on the "Pristine," untreated sample; three different samples that underwent the fluorination procedure at 180°C, 280°C, and 380°C ("PTFE + Heat"); and a sample that underwent the fluorination procedure without PTFE ("Heat Only") at 280°C. A ZEISS Supra 50 VP and Oxford EDS analysis attachment were used for EDS. Using a 15 kV accelerating voltage, three different 10 µm x 10 µm EDS spectra were taken. It is expected that neither the "Pristine" nor the "Heat Only," samples have incorporated fluorine; but the "Heat Only" sample will show the effects

of any heat-induced decomposition. Due to the overlap with the manganese Lα peak (0.637 keV), the fluorine Kα peak (0.677 keV) could not be determined accurately (Figure 7a) [22]. There is no difference between the "Pristine" and the "PTFE + Heat" in Figure 7a. The K/Mn ratio can also be determined from the EDS results (Figure 7b). The relative stability of the K/Mn ratio with heating (from the pristine to the 380ºC fluorinated sample) as shown by EDS agrees with the TGA results (Figure 5). TGA shows that significant decomposition, and thus chemical changes, does not begin until ~600ºC, which is below the fluorination procedure temperature.

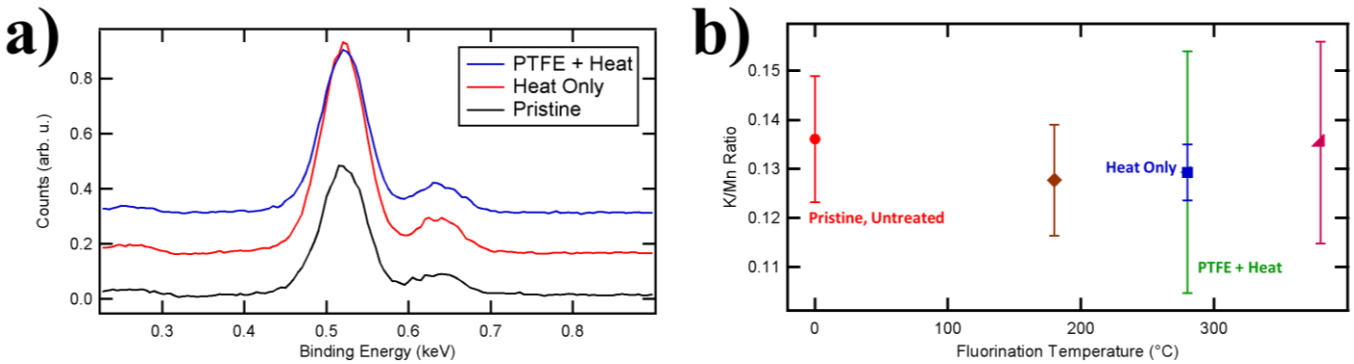

Figure 7. EDS for 4 hour fluorinations **a)** EDS spectra does not allow for fluorine incorporation to be determined due to the overlap between the Mn Lα and F Kα peaks. **b)** The K/Mn ratio is relatively stable with fluorination temperature.

Powder XRD was also performed on the fluorinated samples. All of the fluorinated samples were indexed to the I4/m space group, indicating a topotactic, or structure-preserving, reaction. This is important because the electrochemical properties of α-MnO_2 are derived in large part from its tunnel-like structures. The lattice parameter and unit cell volume show significant changes with fluorination temperature (Figure 8). Because EDS proved unhelpful for determining chemical composition, the discussion is limited to analyzing the unit cell change with fluorination temperature rather than fluorine composition. On a first order discussion, fluorination temperature is a proxy for fluorine incorporation: higher temperatures below the decomposition temperature should lead to higher fluorine incorporation. Other studies using a vapor transport method confirm this approximation by noting an increased fluorine incorporation with increased vapor transport processing temperatures [15], [16].

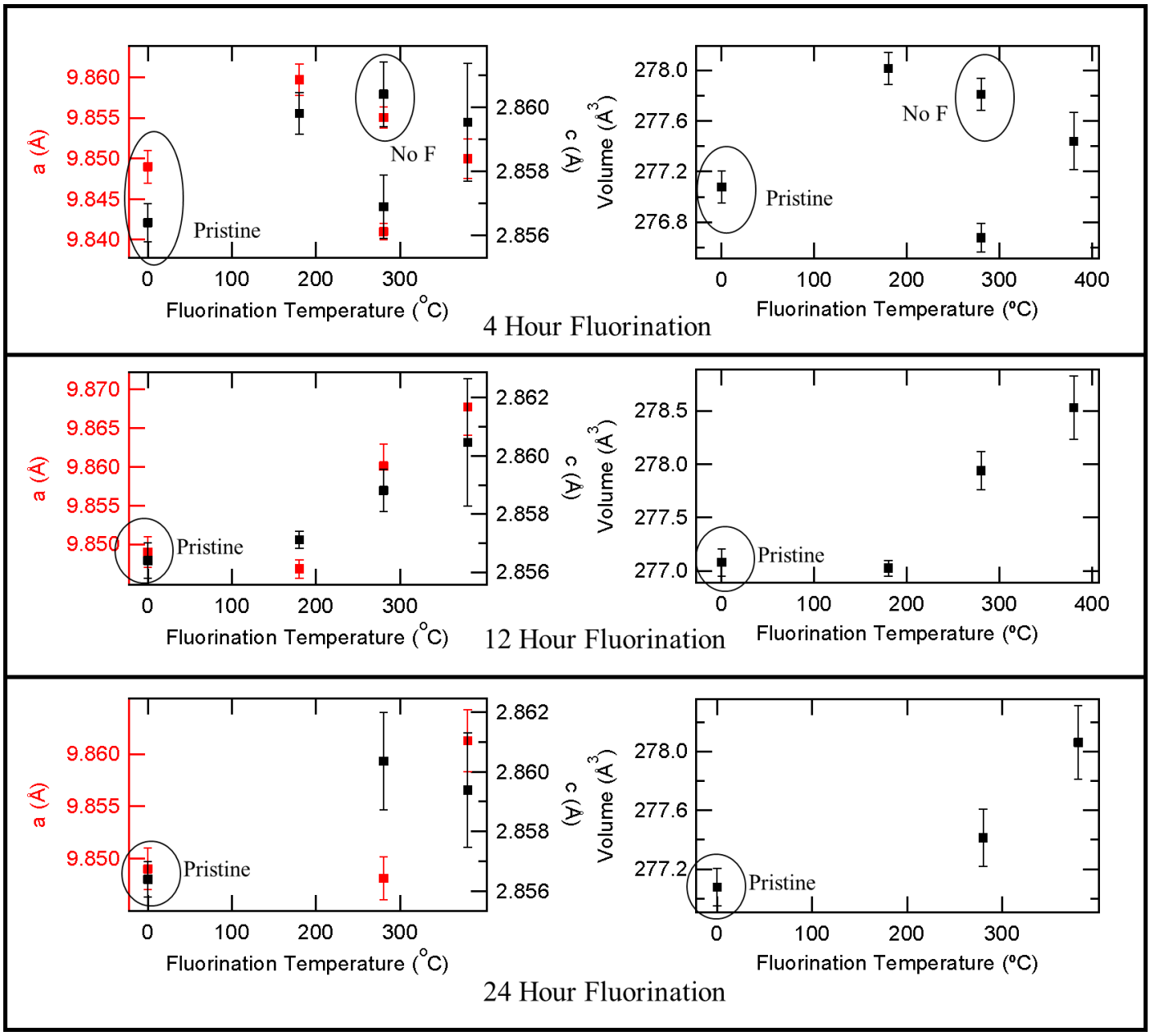

Figure 8. The XRD show that the fluorination process is topotactic. The lattice parameter changes may also be correlated with structural changes due to fluorination.

The incorporation of fluorine can have several effects on the unit cell geometry. These effects include a reductive anion exchange (F^- substitution for O^{2-} accompanied by a reduction of the metal oxide); anion exchange (2 F^- substitute for one O^{2-}); oxidative anion insertion (F^- insertion into interstitial sites accompanied by oxidation of the metal oxide) [23]. For the most part, the fluorination of related layered $LiMO_2$ and spinel $LiMO_4$ (M is a transition metal) has led to an increase in the unit cell volume (Figure 9). In all of these materials, fluorine is reported to

substitute for oxygen rather than incorporate as an interstitial. Furthermore, the ionic radius of fluorine (F^-) is 1.29 Å compared to oxygen (O^{2-}) which has an ionic radius of 1.35 Å [24]. The increase in unit cell volume with the substitution of a smaller ion has been rationalized by a reduction of the transition metal within the metal oxide framework [24]. While others report that the fluorination improves electrode performance, the reduction of manganese from Mn^{4+} to Mn^{2+} or Mn^{3+} could lead to Jahn-Teller distortions, which occurs with Mn^{3+} [8], and manganese dissolution, which occurs with Mn^{2+} [25]. The electrochemical effects of fluorination have yet to be determined, but the complex interplay between structure, atomistic bonding, and macroscopic properties will be of vital importance.

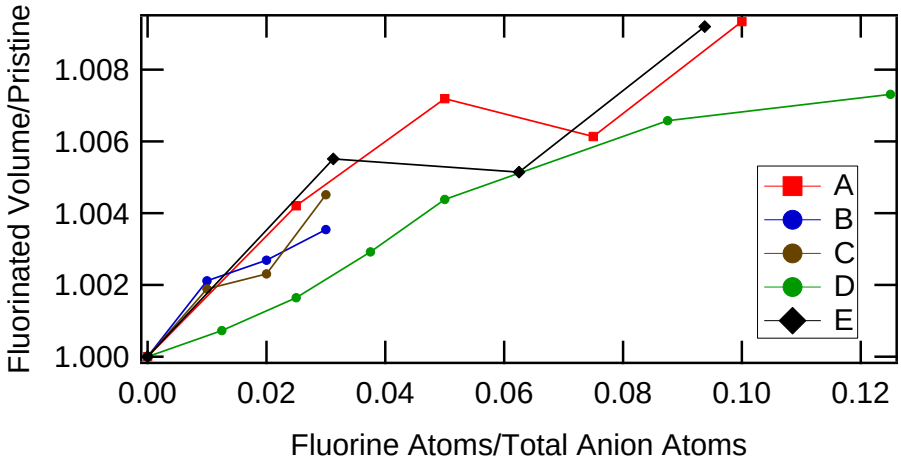

Figure 9. A-E are determined from [9], [17], [26]–[28]. For layered $LiMO_{2-x}F_x$ (M is a transition metal) type materials (A,B, and C), Fluorine Atoms/Total Anion Atoms = x/2. For spinel $LiMO_{4-x}F_x$ type materials (D and E), Fluorine Atoms/Total Anion Atoms = x/4.

The XRD lattice parameter data (Figure 8) indicate that the unit cell volume is increasing with fluorination temperature, which is approximated with fluorine composition. With this, the increasing unit cell volume with fluorine temperature is similar to literature-reported unit cell volume increases for similar manganese oxide based cathode materials. The 4-hour fluorinations (Figure 8, topmost) do not necessarily show this trend as clearly as do the 8-hour and 12-hour processes (Figure 8, middle and bottommost). This indicates that the fluorination process may be kinetically controlled and there may be a threshold time duration for substantial fluorination to be assimilated into the crystal lattice. Still, it must be pointed out that the unit cell volume increase may be due to the removal of retained H_2O within the tunnels [20]. Without chemical composition

data, the full effects of fluorination are difficult to determine and structural changes due to heating and water loss can be easily confounded with those due to fluorine incorporation.

Despite the promising XRD data, it is still imperative to determine whether or not fluorine has actually been incorporated. It has been shown that EDS is not able to distinguish between the manganese and fluorine peaks. To this end, additional techniques such as XPS and atomic absorption spectroscopy (AAS) will be pursued. Future work will also include electrochemical characterization of the cathode materials using galvanostatic cycling tests and using Rietveld analysis to determine the crystallographic orientation of the incorporated fluorine.

Timeline and Upcoming Tasks

As this research project involves many repetitive steps, a traditional Gantt chart is not ideal. The fluorination and material characterization processes will take place continuously as fluorination parameters are changed. Once fluorine introduction has been confirmed via XRD and XPS, electrochemical testing will be performed on the samples. Roughly estimating, fluorination and material characterization will take place throughout the entire Fall Quarter. Electrochemical testing is set to begin during the Winter Quarter. Additionally, magnetic testing will be conducted in winter term.

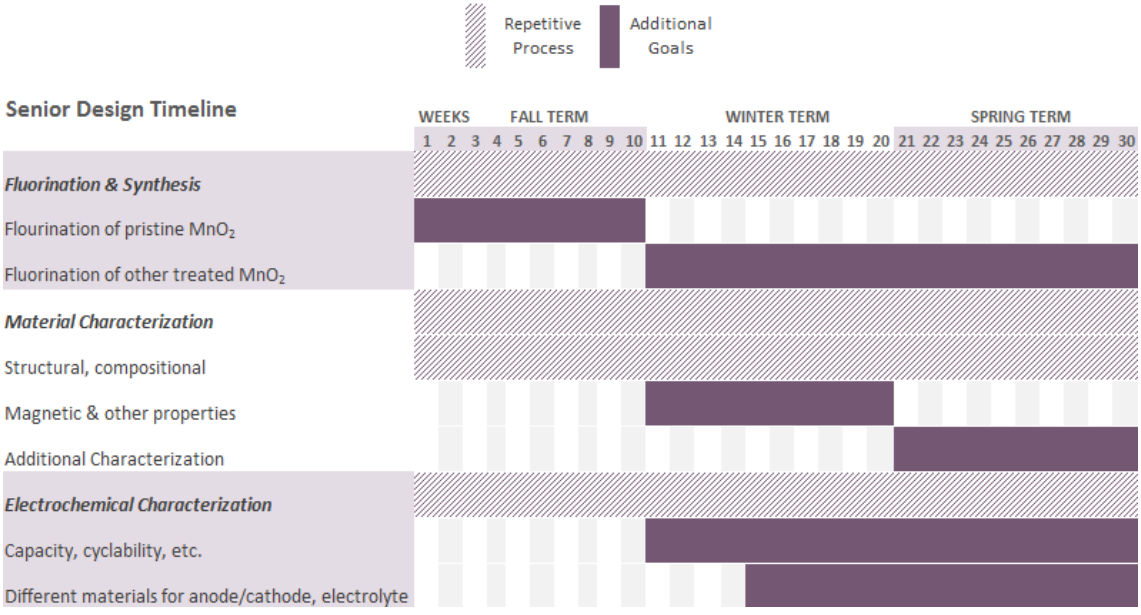

Figure 10. Gantt chart and timeline for project. Hashed purple represent processes which will be repeated through process, solid purple represents tasks with a more fixed time range.

So far, nine fluorinations have been conducted, as noted in Table 1. The two remaining in Table 1 will be conducted in the beginning of winter term. Depending on results, more fluorinations may be conducted at different temperatures or different times, or under repetitive conditions to verify and confirm experimental results. A Gantt chart is displayed in Figure 10.

Additional experimentation may be conducted, time permitting, on the effect of oxygen vacancies through fluorination of acid-leached α-MnO_2. Acid-leaching can induce oxygen vacancies in oxide materials [29]. In fluorination of thin films, it has commonly been seen that oxygen-deficient growth (i.e the presence of oxygen vacancies) allows for increased fluorine insertion [16].

Constraints

So far, the main constraint has been in fluorinations. Due to limited equipment availability of the tube furnace, it has been difficult to conduct more than one fluorination per week, limiting the availability of samples and characterization experiments. This issue will be alleviated, however, by the opening of a fluorination-dedicated fume hood with its own furnace in Winter Term in Lebow 334. There are also some limits on the availability of EDS and XPS, so characterization experiments cannot be performed liberally on all the synthesized materials. Rather, the most promising samples must be identified. Within the synthesis, one major constraint is the fluorination temperature: while high temperatures facilitate greater fluorine incorporation, high temperatures also lead to PTFE and α-MnO_2 decomposition.

For the major components, there have yet to be any other roadblocks: α-MnO_2 synthesis, while time-consuming, has been made in large quantities by the team, and the XRD in the Drexel Centralized Research Facility (CRF) has good time availability. There are no ethical or societal issues posed by this project, and university-outlined lab protocols are being followed to ensure environmental impact is minimal.

Safety Analysis

A full safety analysis of the project was written in early fall term, in which the group discussed the risks pertinent to each task and aspect of the project and the safety measures in place. This report is available by request. All university-outlined safety procedures have been followed

and will to continue to be used throughout the span of the project. The major safety concerns associated with the project are described in Table 2 below. Each safety concern has been accounted for with safety measures.

Briefly though, the largest safety concerns are chemical exposure. Some particularly harmful chemicals include 16 M nitric acid and hydrogen peroxide. The worst-case scenario includes exposure, in which case a safety shower will be used and emergency personnel will be notified. The material synthesis also uses extremely high pressures. A worst-case scenario would resemble last year's (winter of 2016) explosion in the alumni engineering labs. To account for this, special autoclaves with pressure release valves will be used. Throughout the project, the "buddy" system will be used and continual updates of the safety analysis will be performed.

Table 2. Main safety concerns and associated safety measures.

Major process	Sub process	Safety concerns	Safety Measures
Synthesis	Hydrothermal reaction	High pressure reaction	Autoclaves designed with gas release valves
	Chemicals	16 M nitric acid, Hydrogen peroxide	Two layers of nitrile gloves
Fluorination	Fluorine-containing materials (PVDF, PTFE)	Toxicity, Reactivity	Fume Hood, extra hours of flow
	Temperatures up to 400 ^{o}C	High temperatures	Fume hood, insulated gloves, furnace insulation
	Compressed gas cylinders (N_2, Ar, Air)	Compressed Gas	Pressure lock and wall-chain systems
Material Characterization	XRD	X-ray radiation	Sealed shielding door, fail-safe lock
Electrochemical testing	Assembling coin cell	Explosive reaction of lithium with water	Glovebox with controlled humidity
	Electrochemical cycling	Electrical Dangers	Grounded equipment, Warning signs around live circuits
	Lithium-ion Batteries	Short circuiting batteries leading to explosions	Temperature monitoring, Limit charging rates and charging times

Budget

A budget for the project is provided in Table 3. This project is supported by the Materials Electrochemistry Group (MEG, PI: Dr. Ekaterina Pomerantseva) and the Oxide Films & Interfaces Group (OFI, PI: Dr. Steven May) at Drexel University. The materials and equipment to be used for fluorination and testing are readily available through these labs and an XRD subscription has been provided to the group by Dr. May. Any additional expenses incurred are expected to be small and will be provided through the supporting research groups.

Table 3. Expected budget. The "Cost" column is of outright costs for the project, the "Real Cost" considers that many project components are already in use or contained in the supporting lab groups.

	Item	Cost($)	Real Cost ($)	Provider
Lab Supplies	Sample capsules	20	0	OFI
	Quartz tube	50	0	OFI
	Aluminum Foil	10	0	OFI
	Acetone	30	0	OFI
	IPA	30	0	OFI
	Argon Gas	300	55	OFI
	Miscellaneous	20	0	OFI
	PTFE	50	50	OFI
	Subtotal:	***510***	***105***	
Lab Equipment	Tube Furnace	2000	0	OFI
	Autoclave	3000	0	MEG
	Subtotal:	***5000***	***0***	
Equipment Subscription	XRD (Rigaku SmartLab) (9 months)	1000	1000	OFI
	XPS (PHI VersaProbe 5000) (9 months)	3000	0	OFI
	SEM/EDS (Zeiss Supra 50VP, EDAX) (9 months)	2500	0	OFI
	Subtotal:	***6500***	***1000***	
Raw Materials	$KMnO_4$	50	0	MEG
	NH_4Cl	20	0	MEG
	De-ionized Water	30	0	MEG
	Miscellaneous	20	0	MEG
	Subtotal:	120	***0***	
	Total:	***$ 12,130.00***	***$ 1,105.00***	

Conclusion

Here, the details, from the scientific hypotheses to an in-depth overview of budgetary and time constraints, of the proposed project have been thoroughly discussed. Such a review is critical not only for team members to review the current progress and planned goals, but is also useful for graduate advisors and principal investigators to keep apprised of the work.

During the fall quarter, many of the α-MnO_2 samples have been synthesized and fluorinated using the vapor transport method. XRD, SEM, and EDS characterization have been performed to confirm that the correct materials have been synthesized, and that the vapor transport method has thus far maintained the crystal structure of the α-MnO_2. The lattice parameters determined from XRD have shown that the unit cell volume has increased upon the fluorination process. This is in agreement with previously reported data, suggesting that fluorine has successfully been incorporated into the unit cell.

The fluorination process seems to be affected by time and temperature of the processing conditions, suggesting that fluorination is kinetically and thermodynamically controlled. Despite these positive preliminary results, it must be confirmed whether or not fluorine is present within the fluorinated materials. EDS has proven to be unhelpful due to the overlap between the Mn and F peaks. To this end, additional characterization processes such as AAS and XPS will be explored in the winter quarter. In tandem with chemical characterization, the synthesized α-MnO_2 materials will be incorporated into half-cells to test the electrochemical cycling performance. Furthermore, magnetic property testing is planned for the winter quarter.

Overall, a significant amount of progress has been made during the fall quarter, setting the stage for continued momentum in the winter and spring quarters. While the original hypothesis has not yet been proven or disproven, much work remains to be done.

Acknowledgements

The group would like to acknowledge advisors Dr. Steven May and Dr. Ekaterina Pomerantseva and thank both for their advice and efforts through the past term. Mentors Bryan Byles and Jiayi Wang have also been useful in providing instruction and advice on all aspects of this research project. The group would also like to thank the members of the Materials Electrochemistry Group, Oxide Films & Interfaces Group and Centralized Research Facility at Drexel University for their continued support.

References

[1] Y. Dong *et al.*, "Simple hydrothermal preparation of [small alpha]-{,} [small beta]-{,} and [gamma]-MnO2 and phase sensitivity in catalytic ozonation," *RSC Adv.*, vol. 4, no. 74, pp. 39167–39173, 2014.

[2] Brian W. Jaskula, "Lithium," *US Geol. Surv. Miner. Commod. Summ.*, pp. 94–95, 2015.

[3] N. Tanaka, Ed., *Energy Technology Perspectives*. Paris France: International Energy Agency, 2008.

[4] A. Biswal, C. Tripathy, and K. Sanjay, "RSC Advances perspective on worldwide production , reserves and its role in electrochemistry," *RSC Adv.*, vol. 5, pp. 58255–58283, 2015.

[5] B. W. Byles, N. K. R. Palapati, A. Subramanian, and E. Pomerantseva, "The role of electronic and ionic conductivities in the rate performance of tunnel structured manganese oxides in Li-ion batteries," *APL Mater.*, vol. 4, no. 4, p. 46108, 2016.

[6] Y. Cao, L. Xiao, W. Wang, D. Choi, Z. Nie, and J. Yu, "Reversible Sodium Ion Insertion in Single Crystalline Manganese Oxide Nanowires with Long Cycle Life," *Adv. Mater.*, vol. 23, no. 28, pp. 3155–3160, 2011.

[7] B. Sun, Z. Chen, H. Kim, H. Ahn, and G. Wang, "MnO/C core – shell nanorods as high capacity anode materials for lithium-ion batteries," *J. Power Sources*, vol. 196, no. 6, pp. 3346–3349, 2011.

[8] C. S. Johnson *et al.*, "Structural and electrochemical studies of α-manganese dioxide (α-MnO2)," *J. Power Sources*, vol. 68, no. 2, pp. 570–577, 1997.

[9] P. Yue, Z. Wang, H. Guo, X. Xiong, and X. Li, "A low temperature fluorine substitution on the electrochemical performance of layered LiNi0.8Co0.1Mn0.1O2−zFz cathode materials," *Electrochim. Acta*, vol. 92, no. Supplement C, pp. 1–8, 2013.

[10] A. Manthiram, A. V. Murugan, A. Sarkar, and T. Muraliganth, "Nanostructured electrode materials for electrochemical energy storage and conversion," *Energy Environ. Sci*, no. 1, pp. 621–638, 2008.

[11] T. Ohzuku, A. Ueda, M. Nagayama, Y. Iwakoshi, and H. Komori, "Comparative study of LiCoO2, LiNi12Co12O2 and LiNiO2 for 4 volt secondary lithium cells," *Electrochim. Acta*, vol. 38, no. 9, pp. 1159–1167, 1993.

[12] T. Ohzuku and Y. Makimura, "Layered Lithium Insertion Material of LiNi1/2Mn1/2O2 :

A Possible Alternative to LiCoO2 for Advanced Lithium-Ion Batteries," *Chem. Lett.*, vol. 30, no. 8, pp. 744–745, Aug. 2001.

[13] B. Byles, "Unpublished Data." .

[14] Y. Gao, Z. Wang, J. Wan, G. Zou, and Y. Qian, "A facile route to synthesize uniform single-crystalline α-MnO2 nanowires," *J. Cryst. Growth*, vol. 279, no. 3, pp. 415–419, 2005.

[15] E. J. Moon, A. K. Choquette, A. Huon, S. Z. Kulesa, D. Barbash, and S. J. May, "Comparison of topotactic fluorination methods for complex oxide films," *APL Mater.*, vol. 3, no. 6, p. 62511, May 2015.

[16] T. Katayama *et al.*, "Topotactic fluorination of strontium iron oxide thin films using polyvinylidene fluoride," *J. Mater. Chem. C*, vol. 2, no. 27, pp. 5350–5356, 2014.

[17] D. Kim *et al.*, "Full picture discovery for mixed-fluorine anion effects on high-voltage spinel lithium nickel manganese oxide cathodes," *Npg Asia Mater.*, vol. 9, p. e398, Jul. 2017.

[18] W. Choi and A. Manthiram, "Superior Capacity Retention Spinel Oxyfluoride Cathodes for Lithium-Ion Batteries," *Electrochem. solid-state Lett.*, vol. 9, no. 5, pp. 245–248, 2006.

[19] A. N. García, N. Viciano, and R. Font, "Products obtained in the fuel-rich combustion of PTFE at high temperature," *J. Anal. Appl. Pyrolysis*, vol. 80, no. 1, pp. 85–91, 2007.

[20] Z. Yang *et al.*, "Probing the Release and Uptake of Water in α-MnO2·xH2O," *Chem. Mater.*, vol. 29, no. 4, pp. 1507–1517, 2017.

[21] L. Akselrud and Y. Grin, "WinCSD: software package for crystallographic calculations (Version 4)," *J. Appl. Crystallogr.*, vol. 47, no. 2, pp. 803–805, Apr. 2014.

[22] D. E. Newbury, "Misidentification of Major Constituents by Automatic Qualitative Energy Dispersive X-ray Microanalysis: A Problem that Threatens the Credibility of the Analytical Community," *Microsc. Microanal.*, vol. 11, no. 6, pp. 545–561, 2005.

[23] E. E. McCabe and C. Greaves, "Fluorine insertion reactions into pre-formed metal oxides," *J. Fluor. Chem.*, vol. 128, no. 4, pp. 448–458, 2007.

[24] D. Hirai, E. Climent-Pascual, and R. J. Cava, "Superconductivity in WO${}_{2.6}$F${}_{0.4}$ synthesized by reaction of WO${}_{3}$ with teflon," *Phys. Rev. B*, vol. 84, no. 17, p. 174519, Nov. 2011.

[25] B. Xu, D. Qian, Z. Wang, and Y. S. Meng, "Recent progress in cathode materials research for advanced lithium ion batteries," *Mater. Sci. Eng. R Reports*, vol. 73, no. 5, pp. 51–65, 2012.

[26] G.-H. Kim, J.-H. Kim, S.-T. Myung, C. S. Yoon, and Y.-K. Sun, "Improvement of High-Voltage Cycling Behavior of Surface-Modified Li [Ni1/3Co1/3Mn1/3] O2 Cathodes by Fluorine Substitution for Li-Ion Batteries," *J. Electrochem. Soc.* , vol. 152, no. 9, pp. A1707–A1713, Sep. 2005.

[27] P. Yue *et al.*, "The enhanced electrochemical performance of LiNi0.6Co0.2Mn0.2O2 cathode materials by low temperature fluorine substitution," *Electrochim. Acta*, vol. 95, no. Supplement C, pp. 112–118, 2013.

[28] J.-M. T. Glenn G. Amatucci, "Lithium manganese oxy-fluorides for li-ion rechargeable battery electrodes," US5674645 A, 1997.

[29] J. K. Ngala, S. Alia, A. Dobley, V. M. B. Crisostomo, and S. L. Suib, "Characterization and Electrocatalytic Behavior of Layered Li 2 MnO 3 and Its Acid-Treated Form," *Chem. Mater.*, vol. 19, no. 4, pp. 229–234, 2007.

Appendix

Theoretical Capacitance

$$Theoretical\ Capacity\ \left(\frac{Ah}{g}\right) = \frac{F\ \left(\frac{C}{mol}\right)\cdot n}{M\ \left(\frac{g}{mol}\right) * 3600\ \left(\frac{s}{hr}\right)} = 96500\ \frac{A\cdot s}{mol}\cdot 1\cdot\frac{mol}{M\ g}\cdot\frac{1\ hr}{3600\ s}$$
$$= \frac{26.8}{M}(Eq.A1)$$

F is Faraday's constant, n is number of electrons per reaction (1 for lithium), M is molecular weight of electrode material.

For MnO_2, M = 87 g/mol → Theoretical capacity = 308 m-Ah/g
For $LiCoO_2$, M = 100 g/mol → Theoretical capacity = 273 m-Ah /g
For $LiFePO_4$, M = 155 g/mol → Theoretical capacity = 170 m-Ah /g

Error Propagation

Error propagation analysis was used to analyze the error of the XRD and EDS data.

$$f = \frac{A}{B}, \sigma_f = |f|\sqrt{\left(\frac{\sigma_A}{A}\right)^2 + \left(\frac{\sigma_B}{B}\right)^2 - \frac{2\sigma_{AB}}{AB}}\ (Eq.A2)$$

$$f = AB, \sigma_f = |f|\sqrt{\left(\frac{\sigma_A}{A}\right)^2 + \left(\frac{\sigma_B}{B}\right)^2 + \frac{2\sigma_{AB}}{AB}}\ (Eq.A3)$$

A and B are two random variables characterized by variances σ_A^2 and σ_B^2, and a covariance of σ_{AB}.